Hyperspectral Unmixing based on Dual-depth Sparse Probabilistic Latent Semantic Analysis

Ruben Fernandez-Beltran, Antonio Plaza, *Fellow, IEEE*, Javier Plaza, *Senior Member, IEEE*, and Filiberto Pla

***Abstract*—This paper presents a novel approach for spectral unmixing of remotely sensed hyperspectral data. It exploits probabilistic latent topics in order to take advantage of the semantics pervading the latent topic space when identifying spectral signatures and estimating fractional abundances from hyperspectral images. Despite the contrasted potential of topic models to uncover image semantics, they have been merely used in hyperspectral unmixing as a straightforward data decomposition process. This limits their actual capabilities to provide semantic representations of spectral data. The proposed model, called Dual-dEpth probabilistic Semantic Analysis (DEpLSA), makes use of two different levels of topics to exploit the semantic patterns extracted from the initial spectral space in order to relieve the ill-posed nature of the unmixing problem. In other words, DEpLSA defines a first level of deep-topics to capture the semantic representations of the spectra, and a second level of restricted-topics to estimate endmembers and abundances over this semantic space. An experimental comparison in conducted using two standard topic models, and seven state-of-the-art unmixing methods available in the literature. Our experiments, conducted using four different hyperspectral images, reveal that the proposed approach is able to provide competitive advantages over available unmixing approaches.**

***Index Terms*—Hyperspectral unmixing, topic models, probabilistic latent semantic analysis, semantic representations.**

R. Fernandez-Beltran and F. Pla are with the Institute of New Imaging Technologies, University Jaume I, 12071 Castellon, Spain, e-mail: (rufernan,pla)@uji.es.

A. Plaza and J. Plaza are with the Hyperspectral Computing Laboratory, University of Extremadura, 10003 Caceres, Spain, e-mail: (aplaza,jplaza)@unex.es.

I. Introduction

Hyperspectral unmixing (HU) is an essential procedure for Earth and other planetary observations due to the frequent lack of spatial resolution in remotely sensed hyperspectral images [1], [2]. The main goal of HU techniques [3] is decomposing the pixel spectra from a hyperspectral image into a collection of constituent spectral signatures, called *endmembers*, and a set of fractional *abundances*, that indicate the proportion of each endmember present in the pixel. In general, the HU process has proven to be an excellent tool to uncover sub-pixel information from hyperspectral imagery, because endmembers usually correspond to the materials appearing in the scene and, consequently, abundance maps often provide useful information to relieve limited spatial resolutions [4].

A. Brief HU overview

In the literature, it is possible to find two main trends depending on the characterization scale of the HU process [5]: (i) linear and (ii) non-linear models. Whereas the linear HU paradigm assumes that incident light interacts just with one material at a macroscopic scale, the non-linear model takes into account more

complex interactions among the solar radiation scattered by multiple materials in the scene. Despite the potential of non-linear models, many works in the remote sensing field are focused on the linear approach, because common hyperspectral remote sensing sensors usually have a rather limited spatial resolution, what makes reasonable to assume that the mixing process occurs within the instrument itself [6].

Broadly speaking, HU methods can be categorized into three different groups [7]: (a) geometrical, (b) statistical and (c) sparse regression-based. Geometrical methods assume that the endmembers of a hyperspectral image define a simplex of minimum volume enclosing the dataset; therefore the geometry of convex sets can be exploited to identify the simplex vertices [8], [9]. Despite their high computational efficiency, geometrical models tend not to capture highly mixed spectral signatures because simplex facets are often ill-defined with the absence of pure pixels in the scene. In this case, both statistical and regression-based methods provide a more powerful scheme to deal with the HU problem while accounting for endmember variability.

Statistical algorithms make use of a probabilistic framework to infer endmember and abundance parameters as probability distributions which, precisely, are aimed at modeling the data variability. One of the most relevant works was presented by Nascimento and Bioucas in [10], where abundance fractions are defined as mixtures of Dirichlet densities. In other works, the endmember variability is modeled using other kinds of distributions, for instance the Gaussian distribution considered in [11].

Regarding sparse regression approaches, these models formulate the unmixing task as a linear regression problem over a given spectral library [12]. That is, they use a semi-supervised procedure to express the input image as a combination of spectral signatures which are known in advance. Additionally, they usually include some sort of sparsity regularization constraint to refine and alleviate the computational cost of the regression process.

B. Current limitations and trends

Each one of the aforementioned methodologies has shown to be effective under specific conditions. Whereas geometric models are able to produce better endmember estimates when the pure pixel assumption is fulfilled in the scene [7], statistical and regression-based methods tend to obtain a better result in highly mixed scenarios. Nonetheless, statistical models usually lead to computationally demanding algorithms, but they have the advantage of not requiring the availability of a suitable spectral library.

Some recent research lines try to relieve the ill-posed nature of the unmixing problem by taking advantage of so-called *semantic representations* [13], [14], that is, modeling the structural patterns of the spectrum domain. Whereas the traditional hyperspectral image characterization scheme relies on directly using the low level features captured by the spectral bands (e.g. reflectance values), the semantic representation approach pursues to provide a higher level image characterization in which pixels are represented according to the input image spectral patterns. In other words, each pixel is managed as a composition of hyperspectral patterns instead of a collection of raw values. The rationale behind this methodology is based on the fact that spectral patterns can be useful to identify discriminative features in the spectra and, therefore, they can help to reduce the uncertainty when unmixing pixels.

These semantic patterns are often defined in a supervised [15] or semi-supervised form [14] with the collaboration of expert users, who make manual associations between the chemical makeup of materials and the shape of absorption bands in spectral signals.

However, when it comes to unsupervised learning, these patterns usually rely on a regular clustering process [16]. The high complexity of hyperspectral images makes this straightforward approach unable to capture complex spectral relationships, and this eventually limits the semantic power in HU. As a result, additional research is required to improve unmixing techniques under the unsupervised semantic representation research line.

C. Topic models as semantic representations

During the last years, topic models have shown their potential to effectively cope with many kind of tasks by providing data with a higher level of semantic understanding [17]. Text categorization [18], vocabulary reduction [19], image segmentation [20], object recognition [21] or even video retrieval [22] are some of the applications in which the semantic power of topic models have been successfully exploited.

From a practical point of view, latent topics represent a kind of probabilistic models which provide methods to automatically understand and summarize data collections by means of their hidden patterns. In particular, these models are able to express data as probability distributions according to their hidden semantic patterns instead of their low level features, which makes it easier for the data to be managed at a higher abstraction level. Precisely, this is the point that makes topic models an interesting tool to improve the semantic characterization level in HU.

D. Work objectives and main contributions

With the aforementioned considerations in mind, this work is focused on implementing a new perspective on the unsupervised HU statistical approach by means of latent topics [17]. That is, we propose to tackle the unmixing problem as a latent topic-based approach in which endmembers and abundances can be estimated according to the semantics encapsulated by the latent topic space. Several works in the literature advocate the use of topic models for remote sensing applications where the image semantics may be important, such as image annotation [23], scene classification [24], [25] or image super-resolution [26]. Nonetheless, there are few research works within the HU field, and this is precisely the gap that motivates this work. To the best of our knowledge, there is only one work in the literature which relates HU and topic modelling [27]. However, the approach presented here provides a more powerful HU scheme with a comprehensive motivation and a more robust experimental setting to shed light on the general use of topic models within the HU field.

First, we study the straightforward application of standard probabilistic Latent Semantic Analysis (pLSA) [28] and Latent Dirichlet Allocation (LDA) [29] models within the HU field. Later, we propose a new pLSA-based model extension, called Dual-dEpth sparse probability Semantic Analysis (DEpLSA), in order to better adapt the pLSA model to the peculiarities of the unmixing problem. Specifically, we develop a dual-depth pLSA-based architecture using two different levels of topics and a dual entropy-based regularization term to introduce the sparsity constraint, which is also widely taken into account in HU [7]. Finally, we conduct an experimental comparison including some of the most popular HU approaches available in the literature.

The rest of the document is organized as follows: Section II presents the background of the work. In Section III, the proposed DEpLSA model is defined, which is specially adapted to HU. Section IV presents the extended HU framework based on the proposed topic model. Section V shows the experimental part of the work, where seven unmixing methods are tested over four different hyperspectral images. Finally, Section VI discusses the results and Section VII draws the main

conclusions arisen from the work.

II. Background on Topic Models

Topic models [17] can be defined as probabilistic graphical models containing one or more hidden random variables useful to uncover the hidden structure of a data collection. Specifically, given the observed probability distribution $p(w|d)$, which describes a corpus of documents $D = \{d_1,d_2,...,d_M\}$ in a particular word-space $W = \{w_1,w_2,...,w_N\}$, latent topic algorithms are able to obtain two probability distributions: (1) the description of topics in words $p(w|z)$ and (2) the description of documents in topics $p(z|d)$. More specifically, the interpretation that we make of these elements within the HU field is the following: documents (d) are considered hyperspectral image pixels, words (w) are represented by spectral bands, word-counts ($n(w,d)$) contain the pixel-band reflectance values, and topics (z) depict the unmixing process in which probabilities $p(w|z)$ and $p(z|d)$ represent the uncovered endmembers and fractional abundances, respectively.

In general, topic methods can be grouped into two reference families, one based on probabilistic Latent Semantic Analysis (pLSA) [28] and another based on Latent Dirichlet Allocation (LDA) [29]. Specifically, pLSA (Fig. 1a) defines a semi-generative data model by introducing a latent context variable associated to the different word polysemy occurrences. The pLSA generative process is made as follows: (1) Select a document d with probability $p(d)$; (2) Pick a latent class z with probability $p(z|d)$; (3) Generate a word w with probability $p(w|z)$. Nonetheless, this generative process is usually called ill-defined because documents set topic mixtures and simultaneously topics generate documents, thus there is not a natural way to infer previously unseen documents [17].

As a result, Blei et al. proposed the LDA model (Fig. 1b) as a more general framework to overcome pLSA limitations. LDA (Fig. 1b) represents documents as a multinomial of topic mixtures generated by a Dirichlet prior which is able to predict new documents. The LDA generative process can be defined as follows:

1) Choose the length of the document, $N_d \sim Poisson(\xi)$.
2) Choose a parameter vector for the topic distribution, $\theta \sim Dirichlet(\alpha)$. The parameter α is a K-vector (K is the number topics) with components $\alpha_k > 0$ and θ is a K-vector so that $\theta_k \geq 0$ and $\sum_{k=1}^{K}\theta_k = 1$. $p(\theta|\alpha)$ is the probability density function of the Dirichlet distribution.
3) For each one of the N_d words w_n:
    a) Choose a topic $t_n \sim Multinomial(\theta)$.
    b) Choose a word w_n from $p(w_n|t_n,\beta)$, a multinomial probability conditioned on the topic t_n, where β is a $K \times N$ matrix (N is the number of terms in the vocabulary) so that $\beta_{ij} = P(w_j|t_i)$ for all $1 \leq j \leq N$ and $1 \leq i \leq K$.

Although both pLSA and LDA models have shown to be effective in many fields, there are some practical differences that need to be reviewed. The number of pLSA parameters grows linearly with the number of training documents which makes this model particularly memory demanding and susceptible to over-fitting. LDA potentially overcomes these drawbacks by using two Dirichlet distributions, one to model documents $\theta \sim Dir(\alpha)$ and another to model topics $p(w|t,\beta) \sim Dir(\beta)$. However, the α and β hyper-parameters have to be estimated during the topic extraction process and it logically adds an extra computational time and makes LDA performance highly sensitive to the quality of this estimation. In practice, α and β are estimated by

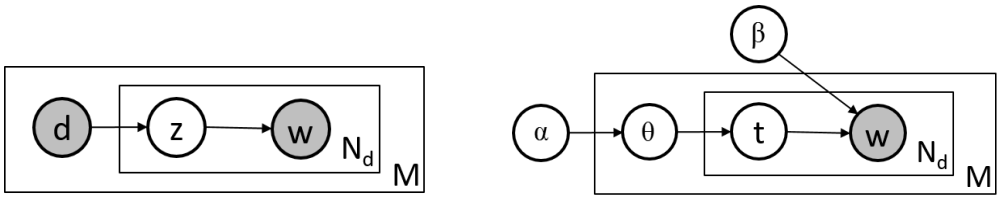

(a) The pLSA topic model.

(b) The LDA topic model.

Fig. 1: In (a), the nodes d,z,w represent document, topic and word random variables. In (b), α and β represent the Dirichlet hyperparameters for the topic-document and word-topic distributions. Besides, θ represents the multinomial distribution generated from the corresponding Dirichlet prior α and t corresponds to the categorical distribution used for the topic activations. In both models, letters N_d and M are the number of words in the document and the total number of documents in the collection. Finally, shaded nodes represent the observable variables of the models.

iterating over the document collection which results in LDA requiring relatively dense distributions to obtain a good hyper-parameter estimation [30]. Even authors in [31] stand that pLSA is able to obtain a topic structure more correlated to the human judgement than LDA, even though the perplexity metric may suggest the opposite. All these facts make pLSA-based models usually preferred when relatively few training samples are available according to the complexity of the problem [31].

In the context of unsupervised HU, the amount of information available to estimate endmembers and abundances is generally rather limited due to the fact that the unmixing process is carried out using only the own input image. As a result, pLSA-based models may take advantage of considering the document collection as model parameters in order to obtain a better spectral semantic characterization than LDA. Ceirtainly, this hypothesis is supported by the fact that, in the unmixing field, it is usual to see approaches based on the Non-negative Matrix Factorization (NMF) [32]–[34] which is, in some sense, connected to pLSA.

The NMF approximation relies on linear algebra to factorize an input matrix into two multiplicative factors in an analogous way to pLSA. Despite the relation between NMF and pLSA [35], there are important implications derived from the pLSA use that can be highly beneficial in HU. First, pLSA offers a highly consistent probabilistic framework to develop further model extensions [3]. Second, pLSA parameters represent probability distributions whereas NMF factors are simply a set of values as vectors or arrays. This fact is especially relevant in HU because the estimation of fractional abundances directly fits into this probabilistic nature. Besides, it also allows evaluating the importance of the estimated endmembers as semantic patterns. Third, pLSA topic-word distributions $p(w|z)$ are identifiable in the vocabulary of mixture models, unlike NMF factors. This has some implications on the theoretical properties of the pLSA Maximum Likelihood estimator, such as a strong consistency [36].

All in all, pLSA offers a more convenient framework than NMF and this is precisely the reason why the HU model we propose in this paper is based on pLSA. Additionally, note that the way we use pLSA and LDA for the HU problem is by assuming that endmembers correspond to topic-word distributions, i.e $p(w|z)$, and abundance factors can be estimated according to the

model by document-topic distributions, i.e. $p(z|d)$.

In addition to the NMF approach, different kinds of unmixing models have been also proposed in the recent literature. For instance, Yang *et al.* present in [37] a novel abundance estimation algorithm based on the bilinear mixture model, which constructs a group of hyperplanes in the low-dimensional feature space to reduce computational complexity. Other works, such as [38], take advantage of a modified Gaussian model to investigate the mineralogical extraterrestrial soil composition. Halimi *et al.* propose in [39] two novel hyperspectral mixture models which account for the presence of nonlinearities by considering a residual term in addition to the linear mixture of endmembers with the sum-to-one and non-negativity abundance constraints. In addition, Yong *et al.* define in [40] a robust sparse unmixing method which simultaneously handles noise and outliers by adopting a $l_{2,1}$ norm loss function.

When considering all these recent methods, the proposed approach is mainly different in three aspects. First, the proposed model is focused on the generative process of the data rather than defining a specific unmixing model equation. Logically, both concepts are related since the data eventually contains the result of the unmixing process, but it is important to highlight that the generative approach itself provides a more complete framework than considering a specific mixing equation because the sum-to-one and non-negativity properties of fractional abundances are inherently incorporated. Second, the proposed approach does not consider any kind of prior distribution but only the own data, which eventually simplifies the complexity of the model when compared to other Bayesian approaches that assume prior distributions with some hyperparameters [41], [42]. Third, the proposed approach is able to estimate both endmembers and fractional abundances, whereas many of the existing Bayesian methods available in the literature [43], [44] are only focused on estimating abundances from a given set of spectral signatures, that is, they deal with the unmixing problem from a semi-supervised perspective whereas the proposed approach does not make use of a spectral library.

III. Dual-depth sparse probabilistic Semantic Analysis

The starting point of the proposed DEpLSA model is the asymmetric formulation of pLSA (Fig. 1a), where a latent topic z is chosen for each document d conditionally to the $p(z|d)$ probability distribution and then a word w is generated from that topic according to $p(w|z)$. The proposed model extension introduces a new latent variable z' in order to create a new level of topics when connecting documents d and words w. Additionally, we introduce two diverging regularization factors, i.e. δ_d and δ_z, to guarantee a dual sparsity constraint when estimating both abundances and endmembers represented by $p(z|d)$ and $p(w|z)$ parameters in the model. Hereinafter, we use the terms *deep-topic* and *restricted-topic* to identify z' and z respectively. Fig. 2 shows the DEpLSA graphical model representation where shaded nodes represent visible random variables.

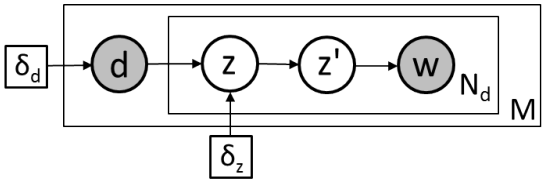

Fig. 2: The proposed DEpLSA topic model. The nodes d,z,z',w represent document, restricted-topic, deep-topic and word random variables. N_d is the number of words in d and M is the total number of documents in the collection. Finally, δ_d and δ_z represent the sparsity factors for documents and restricted-topics respectively.

Likewise in pLSA, the DEpLSA generative process can be described as follows:

1) A document d is chosen from $p(d)$ probability distribution.
2) For each one of the N_d words in the document d,
    a) A restricted-topic z is chosen according to conditional distribution $p(z|d)$ that expresses documents in restricted-topics.
    b) A deep-topic z' is chosen according to conditional distribution $p(z'|z)$ which encapsulates the relation between both levels of topics.
    c) Finally, a word w is chosen according to conditional distribution $p(w|z')$ which expresses deep-topics in words.

The rationale behind the use of DEpLSA in HU is based on using the deep-topics z' to generate the semantic representations of the input spectral data, and then using the restricted-topics z to learn endmembers and abundances in this semantic space. That is, the deep latent space $p(z|z')$ initially projects the original spectra, defined by the visible words w, onto a high dimensional space of K' topics in order to unfold the semantic patterns of the input data. Then, K restricted-topics can be learnt at a higher semantic level to uncover the K endmembers, i.e. $p(w|z)$, and the corresponding abundance maps, i.e. $p(z|d)$. The main difference between z' and z random variables lies in two factors, the space dimensionality and the δ_d and δ_z sparsity constraints. That is, the deep-topic space projects the data onto a high-dimensional space ($K' >> K$) in order to capture fine semantic image patterns of the spectral data. Then, the restricted-topic space takes advantage of these patterns to conduct the unmixing process by fixing the number of restricted topics to the number of endmembers. The use of z' is motivated by the fact that the deep-topic space allows extracting endmembers and abundaces over a semantic characterization space instead of the original spectra. In other words, this high-dimensional space enables connections among spectral signatures through the image patterns defined by topics, and therefore it is able to generate a higher abstraction level for the unmixing process.

In addition, the proposed model makes use of two regularization factors to introduce some sparsity constraints over $p(z'|z)$ and $p(z|d)$ probability distributions in order to reduce the uncertainty and noise. On the one hand, δ_z aims at sparsing the $p(z'|z)$ distribution, which defines the probability of the deep-topics z' given the restricted-topics z. Note that the number of deep topics (K') is significantly higher than the number of endmembers (K), therefore it is reasonable to assume that each endmember (restricted-topic) is modeled using only a limited number of deep-topics. In a sense, this assumption is analogous to the one considered by other sparse coding-based methods, such as [45], [46], to reduce the uncertainty when choosing endmembers from a given spectral library. Logically, the proposed method does not require any spectral library but it can also take advantage of this sparsity constraint over the deep-topic space. On the other hand, the δ_d factor intends to reduce the entropy of the $p(z|d)$ distribution in order to guarantee a better model convergence. That is, the uniform distribution $1/K$ is the most uninformative (highest entropy) abundance map configuration from an information theory perspective and precisely this regularization pursues to encourage sparser and more informative abundance map solutions. In other words, the δ_d regularization aims at neglecting noisy components among the spectral patterns present in a specific pixel (document). This strategy is also common in the sparse-coding field to deal with the input noise, e.g. [47], and this is precisely the reason why we make use of it.

A. Model relaxation

The proposed model takes advantage of two different levels of topics to connect d and w random variables, however this fact has an important implication related to the model inference cost: an additional freedom degree is required to capture the relationships between z and z' hidden random variables. From a pLSA-based perspective, this additional level may become unaffordable as the input image size increases, because each variable marginalization over the posterior distribution requires to evaluate the Cartesian product between z and z'. As a result, in order to alleviate the computational cost of managing two different level of topics when estimating the model parameters, we propose to apply the following model relaxation based on two sequential steps:

1) **Learning deep-topics z' (DEpLSA-1)**: In the first phase (Fig. 3a), the proposed DEpLSA model is simplified to estimate the deep-topic space using a regular pLSA approach. Specifically, components z, δ_d and δ_z are removed from the model in order to approximate the deep-topic distribution, i.e $p(w|z')$, directly from the observable input documents d. As Fig. 3a shows, the DEpLSA-1 model relaxation corresponds to the inner part of DEpLSA and it is equivalent to the standard pLSA model. Therefore, parameters $\Phi' \sim p(z'|d)$ and $\Theta' \sim p(w|z')$ can be initially estimated using pLSA over the input hyperspectral image in order to extract K' deep-topics.
2) **Learning restricted-topics z (DEpLSA-2)**: Once parameters Φ' and Θ' have been estimated, the outer part of DEpLSA corresponds to a dual sparse pLSA model where the random variable related to the deep-topics z' becomes observable as Fig. 3b shows. In particular, we use the parameter Φ' of DEpLSA-1 as the input word-document distribution for DEpLSA-2, i.e. $n(d,z') \approx \Phi'$. Note that this assumption implies considering a uniform prior probability over deep-topics, which is a quite general premise, however different prior probability values could be also used instead to encourage specific topics. Eventually, the $\Phi \sim p(z|d)$ and $\Theta \sim p(z'|z)$ parameters of the DEpLSA-2 model are estimated using K restricted-topics which represent the number of endmembers in the input scene.

This model relaxation allows reducing the DEpLSA computational cost to the pLSA order. Since the DEpLSA-1 model relaxation corresponds to the standard pLSA formulation [28], in the following section we only provide the formulation for the DEpLSA-2 model.

B. Expectation-Maximization formulation for DEpLSA-2

DEpLSA-2 parameters, Φ and Θ, are estimated by maximizing the complete log-likelihood using the Expectation-Maximization (EM) algorithm [48]. First, let us define the likelihood function in terms of the density function of a document collection D,

$$\mathcal{L} = p(D|\Phi,\Theta) = \prod_{d}^{D}\prod_{z'}^{N_{k'}} p(z',d) = \prod_{d}^{D}\prod_{z'}^{K'} p(z',d)^{n(z',d)}, \quad (1)$$

where $N_{k'}$ represents the total number of deep-topics required to generate the document d, K' is the considered number of deep-topics and $n(z',d)$ denotes the number of times the deep-topic z' occurs in the document d. The joint probability $p(z',d)$ can be factorized according to the DEpLSA-2 model as follows:

$$p(z',d) = \sum_{z}^{K} p(z'|z)p(z|d)p(d) = p(d)\sum_{z}^{K} p(z'|z)p(z|d). \quad (2)$$

Note that K represents the number of considered restricted-topics. Inserting Eq. (2) in Eq. (1), we obtain the expression of the complete likelihood:

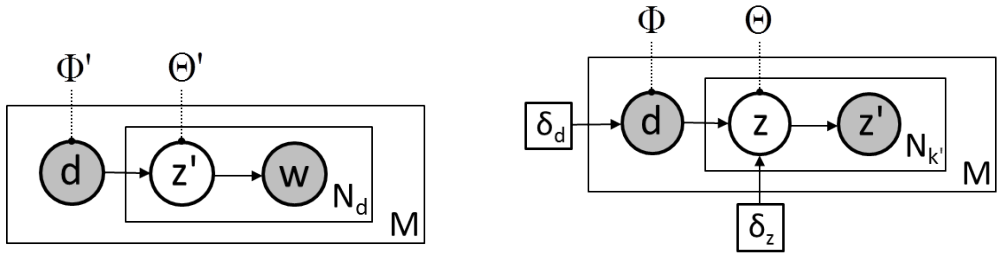

(a) DEpLSA-1, first phase model relaxation.

(b) DEpLSA-2, second phase model relaxation.

Fig. 3: Two-phase model relaxation for the proposed DEpLSA model. See Fig. 2 for notation details.

$$\mathcal{L}_c = \prod_{d}^{D}\prod_{z'}^{K'}\left(p(d)\sum_{z}^{K}p(z'|z)p(z|d)\right)^{n(z',d)}. \quad (3)$$

The target is to estimate the $\Phi \sim p(z|d)$ and $\Theta \sim p(z'|z)$ parameters which maximize the complete likelihood function $\mathcal{L}_c$, nonetheless multiplicative and exponential factors are hard to optimize. Due to the monotonic nature of the logarithmic function, we can equivalently maximize the complete log-likelihood (Eq. (4)) remaining the optimisation problem as Eq. (5) shows:

$$\ell_c = \log(\mathcal{L}_c) = \sum_{d}^{D}\sum_{z'}^{K'}n(z',d)\log\left(p(d)\sum_{z}^{K}p(z'|z)p(z|d)\right), \quad (4)$$

$$\underset{\Phi,\Theta,}{\operatorname{argmax}}\sum_{d}^{D}\sum_{z'}^{K'}n(z',d)\log\left(p(d)\sum_{z}^{K}p(z'|z)p(z|d)\right). \quad (5)$$

Even though the performed simplifications, this expression is still hard to maximize because of the summation inside the logarithm. Taking advantage of the log function properties, we can make use of the concave version of the Jensen's inequality as follows,

$$\sum_{d}^{D}\sum_{z'}^{K'}n(z',d)\log\left(p(d)\sum_{z}^{K}p(z'|z)p(z|d)\right) \geq \sum_{d}^{D}\sum_{z'}^{K'}n(z',d)p(d)\sum_{z}^{K}p(z|z',d)\log(p(z'|z)p(z|d)). \quad (6)$$

As a result, the expression to optimize remains as follows:

$$\mathbb{E} = \sum_{d}^{D}\sum_{z'}^{K'}n(z',d)p(d)\sum_{z}^{K}p(z|z',d)\log(p(z'|z)p(z|d)). \quad (7)$$

Let us now introduce the normalization constraints for parameters $p(z|d)$ and $p(z'|z)$ by inserting the appropriate Lagrange multipliers α and β:

$$\begin{aligned}\mathbb{H}_0 &= \mathbb{E} + \sum_{z}^{K}\alpha\left(1-\sum_{z'}^{N}p(z'|z)\right) \\ &+ \sum_{d}^{D}\beta\left(1-\sum_{z}^{K}p(z|d)\right). \quad (8)\end{aligned}$$

Finally, the solution is regularized using the dual sparsity factors δ_d and δ_Z to maximize the Kullback-Leibler (KL) divergence between the uniform distribution over documents ($U_d = 1/D$) and restricted-topics ($U_z = 1/K$) with respect to parameters $p(z|d)$ and $p(z'|z)$ respectively:

$$\begin{aligned}\mathbb{H} &= \mathbb{H}_0 + \sum_{d}^{D}\delta_d(\mathrm{KL}(U_d|p(z|d))) \\ &+ \sum_{z}^{K}\delta_z(\mathrm{KL}(U_z|p(z'|z))) \\ &= \mathbb{H}_0 - \sum_{d}^{D}\delta_d\left(\frac{1}{K}\sum_{z}^{K}\log(p(z|d))\right) \\ &- \sum_{z}^{K}\delta_z\left(\frac{1}{N}\sum_{z}^{K}\log(p(z'|z))\right). \quad (9)\end{aligned}$$

To maximize the above expression, we use the EM algorithm which works in two stages: (i) E-step, where given the current estimation of the parameters the expected value of the likelihood is computed (estimating the posterior probability $p(z|z',d)$) and (ii) M-step, where the new optimal values of the parameters are computed according to the current setting of the hidden variables.

For the M-step, we calculate Eq. (9) partial derivatives, set them equal to zero and solve the equations to estimate $p(z'|z)$ (Eq. (10)) and $p(z|d)$ (Eq. (11)) parameters. Note that α and β multipliers can be obtained from the normalization constraint on topics and documents, respectively.

$$p(z'|z) = \frac{\sum_d n(z',d)p(d)p(z|z',d) - \delta_z/K'}{\sum_{z'}\sum_d n(z',d)p(d)p(z|z',d)} \quad (10)$$

$$p(z|d) = \frac{\sum_{z'} n(z',d)p(z|z',d) - \delta_d/K}{\sum_z \sum_{z'} n(z',d)p(z|z',d)} \quad (11)$$

For the E-step, $p(z|z',d)$ probabilities can be computed by applying the Bayes' rule and the chain rule as Eq. (12) shows.

$$p(z|z',d) = \frac{p(z',d,z)}{p(z',d)} = \frac{p(z',d,z)}{\sum_z p(z',d)} = \frac{p(z'|z)p(z|d)}{\sum_z p(z'|z)p(z|d)} \quad (12)$$

The EM process is performed as follows. First, $p(z|d)$ and $p(z'|z)$ are randomly initialized. Then, the E-step (Eq. (12)) and the M-step (Eqs. (10)-(11)) are alternated until $p(z'|z)$ and $p(z|d)$ parameters converge. As convergence conditions, we use a 10^{-6} stability threshold in the difference of the log-likelihood (Eq. (4)) between two consecutive iterations and a maximum number of 1000 EM iterations.

IV. HU FRAMEWORK BASED ON DEPLSA

In order to enable the use of LDA, pLSA and DEpLSA models over HS images, we make use of the Bag-of-Words (BoW) characterization scheme [49] adapted to the spectral image domain. Specifically, pixels are considered as topic model documents, spectral bands define the vocabulary terms and document word-counts are represented by the reflectance values of the bands. Note that considering an image size of $(r \times c \times b)$, this characterization generates a total of $D = (r \times c)$ documents with a $N = b$ vocabulary size.

Fig. 4 shows a general overview of the proposed HU framework based on the DEpLSA model. From left to right, the proposed methodology consists of three sequential steps: (1) learning the deep-topic space, (2) extracting the restricted topics and (3) generating the output endmemember signatures and abundance maps.

Once the input HS image is characterized as a collection of spectral documents, the first step is based on applying the DEpLSA-1 model to learn the deep-topic space using K' latent units. Note that this step aims at obtaining a high dimensional deep-topic space to unfold semantic patterns of the original spectral data, therefore the number of deep-topics K' has to be substantially higher than the vocabulary size N.

In the second step (2), the DEpLSA-2 model is used to extract K restricted topics over the deep-topic space previously learnt. That is, the $\Phi' \sim p(z'|d)$ parameter of DEpLSA-1 acts as the input word-document distribution for DEpLSA-2 in order to uncover K endmembers considering δ_d and δ_z sparsity factors.

Finally, the third step (3) is focused on obtaining the final endmember and abundance results. The $\Phi \sim p(z|d)$ parameter of DEpLSA-2 provides a direct estimate of the fractional abundances due to the fact that it expresses pixels according to the probability of belonging to each

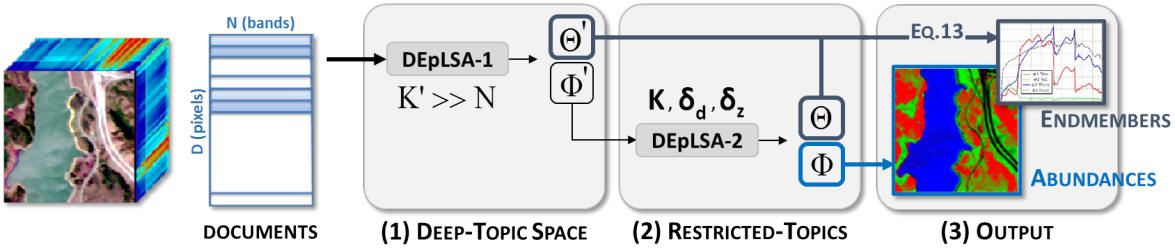

Fig. 4: Overview of the proposed HU framework.

one of the K endmembers. However, the considered model relaxation (Sec. III-A) does not provide any straightforward endmember estimation. In order to obtain such result, we approximate it by factorising the $p(w|z)$ probability as follows:

$$p(w|z) = \frac{p(w,z)}{p(z)} = \sum_{z'} \overbrace{p(w|z')}^{\text{DEpLSA-1}} \overbrace{p(z'|z)}^{\text{DEpLSA-2}} = \Theta'\Theta. \quad (13)$$

Note that the $p(w|z)$ distribution represents the K restricted-topics in the initial vocabulary space of spectral bands, therefore it provides an estimation of the spectral signatures. In particular, we initially factorize $p(w|z)$ according to the proposed DEpLSA model (Sec. III). Then, the Θ' and Θ parameters can be used to connect both the deep-topic space and the restricted-topic space estimated by the DEpLSA-1 and DEpLSA-2 models, respectively.

V. Experimental Results

The experimental part of the work aims at validating the performance of LDA, pLSA and DEpLSA models within the HU field against several unmixing algorithms available in the literature. In particular, Section V-A introduces the five hyperspectral images used in the experiments, Section V-B describes the experimental setting and Section V-C shows the obtained results.

A. Datasets

We have considered five different hyperspectral datasets in our experiments, one synthetic image, called Fractal [50], and four real hyperspectral images, which are Samson, Jasper, Urban and Cuprite datasets [51]. These images have been selected because they are used in many recent works [52]–[55] and also because they are publicly available and can be easily donwloaded from websites [56], [57]. In the following, we provide a description of all the considered hyperspectral data sets.

1) Fractal (Fig. 5a) [50] is a simulated hyperspectral image which has 221 spectral bands and its size in pixels is 100×100. It contains a total of 9 endmember mineral signatures selected from the U.S. Geological Survey (USGS) spectral library, i.e. Alunite, Dumortierite, Halloysite, Kaolinite1, Kaolinite9, Muscovite, Nontronite, Pyrophilite and Sphene, which cover the wavelengths from 400 nm to 2500 nm. Specifically, the procedure for generating this synthetic image, which is detailed in [50], mainly assigns different spectral signatures to adjacent image regions and then it calculates fractional abundances considering pure pixels in each region center and linearly mixed pixels for transitions. In addition to the noise-free version of the Fractal image, three different levels of zero-mean Gaussian noise have been considered [50]: 30 SNR (signal to noise ratio), 50 SNR and 70

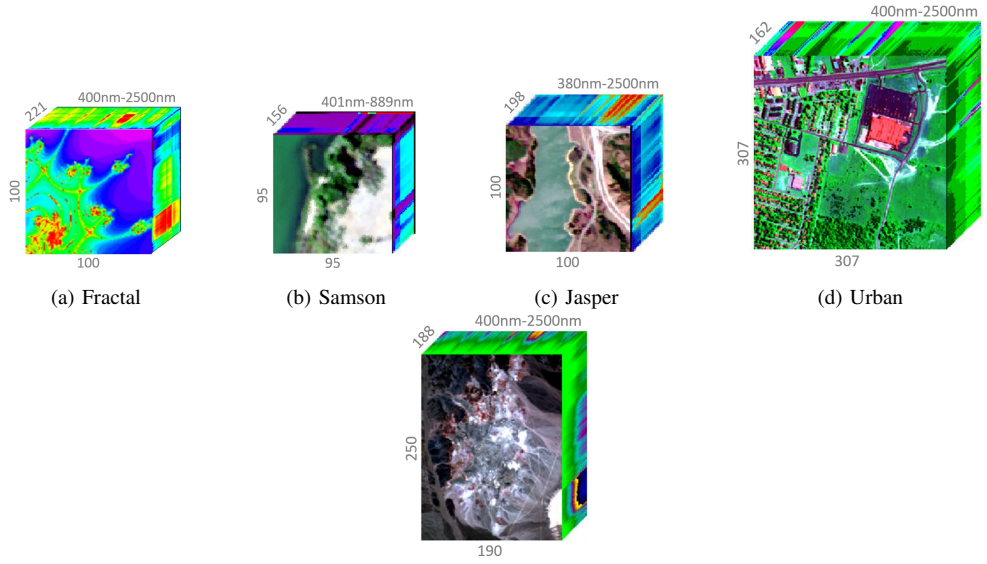

(a) Fractal (b) Samson (c) Jasper (d) Urban

(e) Cuprite

Fig. 5: Hyperspectral images considered in our experiments.

SNR.

2) Samson (Fig. 5b) [51] is a simple hyperspectral image with a size of 952×952 pixels and 156 bands. The spectral resolution is highly up to 3.13 nm and it covers the wavelengths from 401 nm to 889 nm. In order to reduce the computational cost of the tested HU methods, a region of 95×95 pixels has been cropped from the (252,332)-th pixel in the original image. There are three materials present in the image: soil, tree and water.
3) Jasper (Fig. 5c) [51], [58]–[60] is a popular hyperspectral data set which contains 512×614 pixels per band. It has a total of 224 channels with a spectral resolution up to 9.46 nm ranging from 380 nm to 2500 nm. Due to the high complexity of the image, we consider an area of 100×100 pixels starting from the (105,269)-th pixel in the original image. In a addition, channels 1-3, 108-112, 154-166 and 220-224 have been removed to avoid atmospheric effects (198 channels remain). The number of members in this scene is four: road, soil, water and tree.
4) Urban (Fig. 5d) [51], [58]–[60] is another common hyperspectral image present in many HU works. Specifically, it has a size of 307×307 with a spatial resolution of 2 mpp (meter per pixel). There are 210 spectral bands ranging from the 400 nm to the 2500 nm wavelength what results in a spectral resolution of 10 nm. As a pre-processing step, we remove bands 1-4, 76, 87, 101-111, 136-153 and 198-210 to avoid atmospheric effects (162 channels remain). The number of materials in the scene is four: asphalt, grass, tree and roof.
5) Finally, Cuprite (Fig. 5e) [51], [59], [60] is one of the most challenging datasets for HU which covers the Cuprite mining district in NV, U.S. This image contains 224 channels, ranging from 370 nm to 2480 nm. Similarly to the other datasets, a region of 250×190 pixels is considered and we also remove the noisy channels (1-2 and 221-224) and water absorption channels (104-113 and 148-167) in order to maintain a total of 188 chan-

nels. A total of 12 types of minerals are present in the scene: Alunite, Andradite, Buddingtonite, Dumortierite, Kaolinite1, Kaolinite2, Muscovite, Montmorillonite, Nontronite, Pyrope, Sphene and Chalcedony.

B. Experimental settings

The proposed approach has been validated against 9 different methods selected from the literature. In particular, three different families of methods have been included in this experimental comparison: geometrical-based, Non-negative Matrix Factorization-based and latent topic-based. Regarding the first group, the Vertex Component Analysis (VCA) [8] and Minimum Volume Simplex Analysis (MVSA) [9] unmixing methods have been considered. For the second one, four different variations of the standard NMF procedure [61] have been taken into account: NMF-div [62], which uses the Kullback-Leibler divergence criterion to perform the decomposition, NMF-mse [62], which employs an Euclidean objective function, NMF-sp [63], which also introduces a sparsity constraint, and CNMF [34], which uses two different kinds of regularization terms. Finally, three different topic models have been tested for the unmixing problem, LDA [29], pLSA [28] and pLSA-sp [27], which adds a sparsity constraint over documents.

All these methods have been selected because their implementations are publicly available and besides they allow estimating both endmembers and abundances in the same form as the proposed framework does. That is, we assume that the number of endmembers K is known in advance, therefore all the tested methods make use of this information when conducting the unmixing experiments. Note that multiple works in the literature are focused on estimating the number of endmembers, thus some methods like [64] could be used as a pre-processing step to estimate this number.

Whenever possible, the considered methods have been tested using a similar parameter configuration in order to conduct experimental comparisons which are as fair as possible taking into account the approaches' diversity. In particular, the NMF-sc abundance and endmember sparsity constraints have been fixed to 10^{-2} and $1/N$, respectively. Similarly, the pLSA-sp abundance sparse factor has been set to 10^{-2}. Finally, the δ_d and δ_z sparsity factors of the proposed approach have been fixed to 10^{-2} and $1/K'$. Note that for the δ_z term we use $1/K'$ instead of $1/N$ because K' is the vocabulary length of the restricted-topics which is set to 1000 in this work. Regarding the convergence of the algorithms, we have considered a maximum of 1000 iterations for both NMF-based and topic-based models.

In order to perform a quantitative evaluation of the HU results, two reference metrics are used: the Spectral Angle Distance (SAD) and the Root Mean Squared Error (RMSE). On the one hand, the SAD [65] is used to assess endmember estimates by considering each spectral band as a coordinate axis and then computing the average angle between the estimated endmembers $\widetilde{M}$ and the ground-truth ones M. Eq. (14) shows the expression defining this metric, where K represent the number of endmembers.

$$\mathrm{SAD}(\widetilde{\mathbf{M}},\mathbf{M}) = \frac{1}{K}\sum_{i}^{K}\arccos\frac{\widetilde{\boldsymbol{M}}_i \cdot \boldsymbol{M}_i}{||\widetilde{\boldsymbol{M}}_i||\ ||\boldsymbol{M}_i||}. \quad (14)$$

On the other hand, the RMSE metric is useful to evaluate the abundance estimation results by computing the absolute differences between the estimated abundances ($\widetilde{A}$) and the ground-truth ones (A) as eq. (15) shows. Note that R and C represent the input image size.

$$\mathrm{RMSE}(\widetilde{\mathbf{A}},\mathbf{A}) = \sqrt{\frac{1}{R\cdot C}\sum_{i}^{R}\sum_{j}^{C}(\widetilde{A}_{i,j} - A_{i,j})^2}. \quad (15)$$

Regarding the ground-truth information used to compute these metrics, we use the ground-truth data available in [56], [57]. In the case of the simulated image (Fractal), real endmembers and abundances are logically known in advance. For Samson, Jasper and Urban images, we make use of the ground-truth information in [66], which has been obtained using a semi-supervised approach also employed in [67], [68]. First, the VD (Virtual Dimensionality) method [69] is used to find out the number of endmembers. Second, the endmember spectral signatures are manually chosen from the USGS (United States Geological Survey) library[1] and other hyperspectral libraries, according to the acquisition area. Finally, the corresponding fractional abundances are generated by solving the constrained convex optimization also applied in [68]. For the Cuprite dataset, we consider the USGS library signatures of the most representative minerals in the scene, available in [57].

C. Results

Tables I-II show the SAD and RMSE quantitative assessment for the considered unmixing methods and datasets. In the case of the synthetic Fractal data, four different levels of Gaussian noise are considered, i.e. without noise (noNoise), 30 SNR, 50 SNR and 70 SNR. In the case of the real data, four different hyperspectral images are included, i.e. Samson, Jasper, Urban and Cuprite. Regarding the considered unmixing methods, two column groups are differentiated: (A) Non-topic-based methods, i.e. VCA [8], MVSA [9], NMF-div [62], NMF-mse [62], NMF-sp [63] and CNMF [34], and (B) Topic-based methods, i.e. LDA [29], pLSA [28] and pLSA-sp [27] together with the results obtained by the proposed approach. Note that two different columns are shown for the proposed approach: DEpLSA-noReg, that shows the result obtained without regularization (that is, $\delta_d = \delta_z = 0$), and DEpLSA, where the configuration explained in Sec.V-B is used.

In addition to the quantitative evaluation provided by the SAD and RMSE metrics, some visual results are presented as a qualitative evaluation for the tested HU methods. Specifically, Figs. 6-8 show the abundance estimation results for Samson, Jasper and Urban datasets obtained by a subset of the tested methods: VCA, NMF-sp, CNMF, LDA, pLSA, pLSA-sp and the proposed DEpLSA model. Besides, the acronym GT represents the ground-truth abundances. Since for the Cuprite data set there is no GT abundance map that can be used as reference, we do not display the abundance maps in this case. Additionally, Figure 9 provides the Cuprite endmember results and abundance maps for the proposed method.

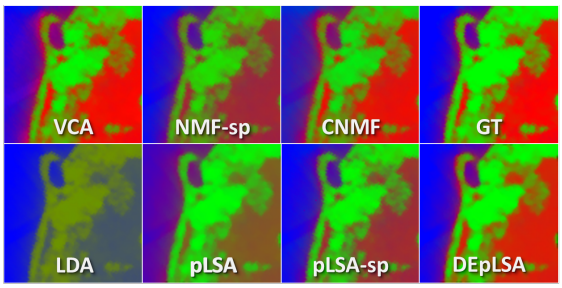

Fig. 6: Samson abundance results for VCA, NMF-sp, CNMF, LDA, pLSA, pLSA-sp and the proposed DEpLSA method. The ground-truth image (GT) is shown at the top-right position. Soil, tree and water endmembers are represented using pure red, green and blue colors, respectively.

VI. Discussion

According to the unmixing results obtained from the synthetic hyperspectral data (Tables I-II), the proposed approach is able to provide a remarkable performance

[1] https://speclab.cr.usgs.gov/

TABLE I: Spectral Angle Distance (SAD) endmember assessment for the considered datasets using different unmixing methods. In rows, the Fractal synthetic dataset with different levels of noise and the four considered real images. In columns, the considered unmixing methods organized in two groups: (A) Non-topic-based methods and (B) Topic-based methods. Note that the shown values correspond to the average and standard deviation radians over endmembers. Besides, results are multiplied by a 10^{-2} factor and the best values for each row and each method group are highlighted in italics and bold font respectively.

Datasets		Members (K)	Spectral Angle Distance - SAD ($\times 10^{-2}$)										
			(A) Non-topic-based methods						(B) Topic-based methods				
			VCA	MVSA	NMF-div	NMF-mse	NMF-sp	CNMF	LDA	pLSA	pLSA-sp	DEpLSA-noReg	DEpLSA
Synthetic data	Fractal (noNoise)	9	0.29 ± 0.3	***0.05 ± 0.06***	21.84 ± 7.45	23.69 ± 8.13	20.11 ± 5.53	0.07 ± 0.08	39.59 ± 7.45	24.77 ± 8.94	14.38 ± 8.18	**1.55 ± 0.84**	1.59 ± 1.08
	Fractal (SNR 30)	9	**4.66 ± 10.3**	9.76 ± 9.58	23.52 ± 7.95	25.48 ± 8.71	22.2 ± 6.23	7.18 ± 8.11	45.25 ± 8.52	30.82 ± 12.02	21.23 ± 13.36	4.56 ± 2.5	***3.24 ± 2.94***
	Fractal (SNR 50)	9	***0.33 ± 0.3***	2.88 ± 3.53	22.78 ± 7.77	24.71 ± 8.49	20.97 ± 5.76	1.3 ± 1.52	42.67 ± 8.03	28.38 ± 10.87	17.95 ± 11.54	2.58 ± 2.3	**1.75 ± 1.13**
	Fractal (SNR 70)	9	0.29 ± 0.3	0.28 ± 0.33	22.15 ± 7.55	24.03 ± 8.25	20.4 ± 5.6	***0.15 ± 0.14***	41.13 ± 7.74	25.78 ± 5.66	15.84 ± 7.87	2.17 ± 1.36	**1.67 ± 1.12**
Real data	Samson	3	**6.33 ± 4.69**	16.32 ± 7.26	13.52 ± 8.93	13.1 ± 9.04	13.1 ± 1.18	11.86 ± 11.71	34.95 ± 22.75	19.27 ± 13.1	12.64 ± 9.63	4.27 ± 1.9	***3.51 ± 1.05***
	Jasper	4	28.39 ± 27.71	28.42 ± 17.58	36.79 ± 21.17	37.56 ± 21.94	**25.7 ± 7.62**	29.35 ± 27.88	36.39 ± 18.94	30.41 ± 4.68	30.07 ± 10.42	15.23 ± 13.06	***11.77 ± 2.25***
	Urban	4	29.41 ± 21.06	34.78 ± 17.55	37.56 ± 20.48	39.26 ± 15.35	**23.95 ± 7.9**	26.86 ± 23.88	40.91 ± 11.84	33.24 ± 18.83	30.91 ± 15.39	13.84 ± 13.41	***8.03 ± 0.9***
	Cuprite	12	**17.94 ± 31.48**	20.93 ± 6.84	40.14 ± 30.41	41.97 ± 31.52	31.54 ± 2.17	21.61 ± 16.71	63.73 ± 29.71	44.57 ± 35.56	26.81 ± 33.3	20.02 ± 31.54	***17.86 ± 14.3***

TABLE II: Root Mean Squared Error (RMSE) abundance assessment for the considered datasets using different unmixing methods. In rows, the Fractal synthetic dataset with different levels of noise and the four considered real images. In columns, the considered unmixing methods organized in two groups: (A) Non-topic-based methods and (B) Topic-based methods. Note that the shown values correspond to the RMSE average and standard deviation over abundance maps. Besides, results are multiplied by a 10^{-2} factor and the best values for each row and each method group are highlighted in italic and bold font respectively. Also note that, for the Cuprite data set, there is no ground-truth abundance map that can be used as reference and, hence, the RMSE metric cannot be computed in this case.

Datasets		Members (K)	Root Mean Squared Error - RMSE ($\times 10^{-2}$)										
			(A) Non-topic-based methods						(B) Topic-based methods				
			VCA	MVSA	NMF-div	NMF-mse	NMF-sp	CNMF	LDA	pLSA	pLSA-sp	DEpLSA-noReg	DEpLSA
Synthetic data	Fractal (noNoise)	9	8.67 ± 1.86	21.82 ± 4.71	17.46 ± 2.51	17.44 ± 2.58	17.01 ± 3.01	***0.15 ± 0.11***	14.99 ± 2.69	15.86 ± 2.49	15.68 ± 2.74	**3.96 ± 2.09**	3.99 ± 1.86
	Fractal (SNR 30)	9	20.48 ± 4.19	22.71 ± 4.6	17.51 ± 2.53	17.48 ± 2.61	16.83 ± 3.07	**9.68 ± 1.5**	17.14 ± 3.08	19.03 ± 3.41	19.09 ± 1.81	10.07 ± 3.06	***7.91 ± 4.01***
	Fractal (SNR 50)	9	8.65 ± 1.86	22.37 ± 3.82	17.47 ± 2.51	17.44 ± 2.59	17.01 ± 3.01	***1.42 ± 0.24***	16.16 ± 2.9	18.35 ± 3.06	17.23 ± 3.38	5.14 ± 2.69	**5.03 ± 2.43**
	Fractal (SNR 70)	9	8.59 ± 1.85	22.27 ± 4.38	17.46 ± 2.51	17.44 ± 2.58	17.01 ± 3.01	***0.22 ± 0.09***	15.57 ± 2.8	18.09 ± 3.35	15.84 ± 3.2	4.98 ± 2.12	**4.13 ± 1.9**
Real data	Samson	3	18.26 ± 0.57	37.99 ± 5.92	13.92 ± 2.39	14.63 ± 2.93	13.82 ± 0.42	**12.33 ± 0.09**	27.73 ± 8.69	19.51 ± 6.06	12.68 ± 4.46	5.49 ± 1.83	***4.78 ± 2.02***
	Jasper	4	29.88 ± 3.01	38.8 ± 11.13	22.02 ± 1.99	22.52 ± 2.06	**15.62 ± 2.06**	26.3 ± 8.72	21.61 ± 5.92	24.47 ± 0.84	20.36 ± 5.2	15.56 ± 4.64	***12.04 ± 1.59***
	Urban	4	24.49 ± 4.12	30.44 ± 6.03	19.5 ± 1.54	21.37 ± 2.36	**12.84 ± 1.16**	23.07 ± 4.03	21.24 ± 7.01	17.48 ± 4.79	15.47 ± 3	13.65 ± 4.69	***11.97 ± 1.15***
	Cuprite	12	-	-	-	-	-	-	-	-	-	-	-

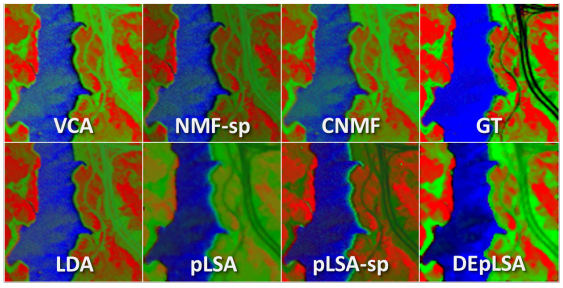

Fig. 7: Jasper abundance results for VCA, NMF-sp, CNMF, LDA, pLSA, pLSA-sp and the proposed DEpLSA method. The ground-truth image (GT) is shown at the top-right position. Tree, soil, water and road endmembers are represented using pure red, green, blue and black colors, respectively.

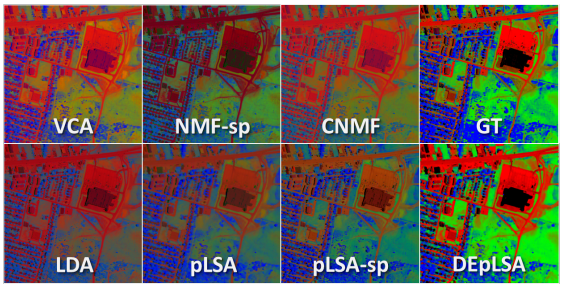

Fig. 8: Urban abundance results for VCA, NMF-sp, CNMF, LDA, pLSA, pLSA-sp and the proposed DEpLSA method. The ground-truth image (GT) is shown at the top-right position. Asphalt, grass, tree and roof endmembers are represented using pure red, green, blue and black colors, respectively.

improvement with respect to the rest of the tested methods when considering a certain amount of input noise. That is, DEpLSA obtains the best SAD and RMSE values for Fractal 30 SNR and the second and third best average quantitative result for Fractal 50 SNR, which indicates the good performance of the proposed approach under noisy conditions. Nonetheless, it is also possible to observe that other methods, especially CNMF, tend to obtain better results in a low-level noise scenario (Fractal 70 SNR) and in free-noise conditions (Fractal noNoise). Note that the non complex nature of the simulated data makes that pure pixels can easily occur when not considering noise or a small amount of it, therefore straightforward methods may generate a more accurate unmixing estimates than the proposed approach probabilistic nature. However, the absence of noise is not a realistic premise in a real remotely sensed hyperspectral data production scenario where images are typically affected by many different kinds of perturbations and image corrections that introduce some noise as well. Precisely, this is the reason why we also use real hyperspectral data in the experimental part of the work.

The quantitative assessment reported in Tables I-II reveals that the proposed DEpLSA model is able to achieve a competitive HU performance with the four real considered hyperspectral datasets. When considering the SAD metric (Table I), the proposed approach shows a remarkable reduction on the angular deviation between the estimated endmembers and the ground-truth ones. Although the geometrical method (VCA) and the NMF-based one (CNMF) also exhibit good capabilities to extract endmembers, the result provided by DEpLSA tends to be more accurate as well as robust. That is, whereas VCA and CNMF decrease their effectiveness for Jasper and Urban datasets, the proposed approach is able to maintain a good performance for all the considered hyperspectral images.

In the case of the RMSE metric, it is possible to identify a similar behaviour. More specifically, DEpLSA achieves the best results and the second best average value is obtained by NMF-sp. Nonetheless, the performance of the proposed approach remains significantly higher on average. According to the reported results, we can also see that VCA and CNMF are certainly less effective to estimate abundances than to estimate

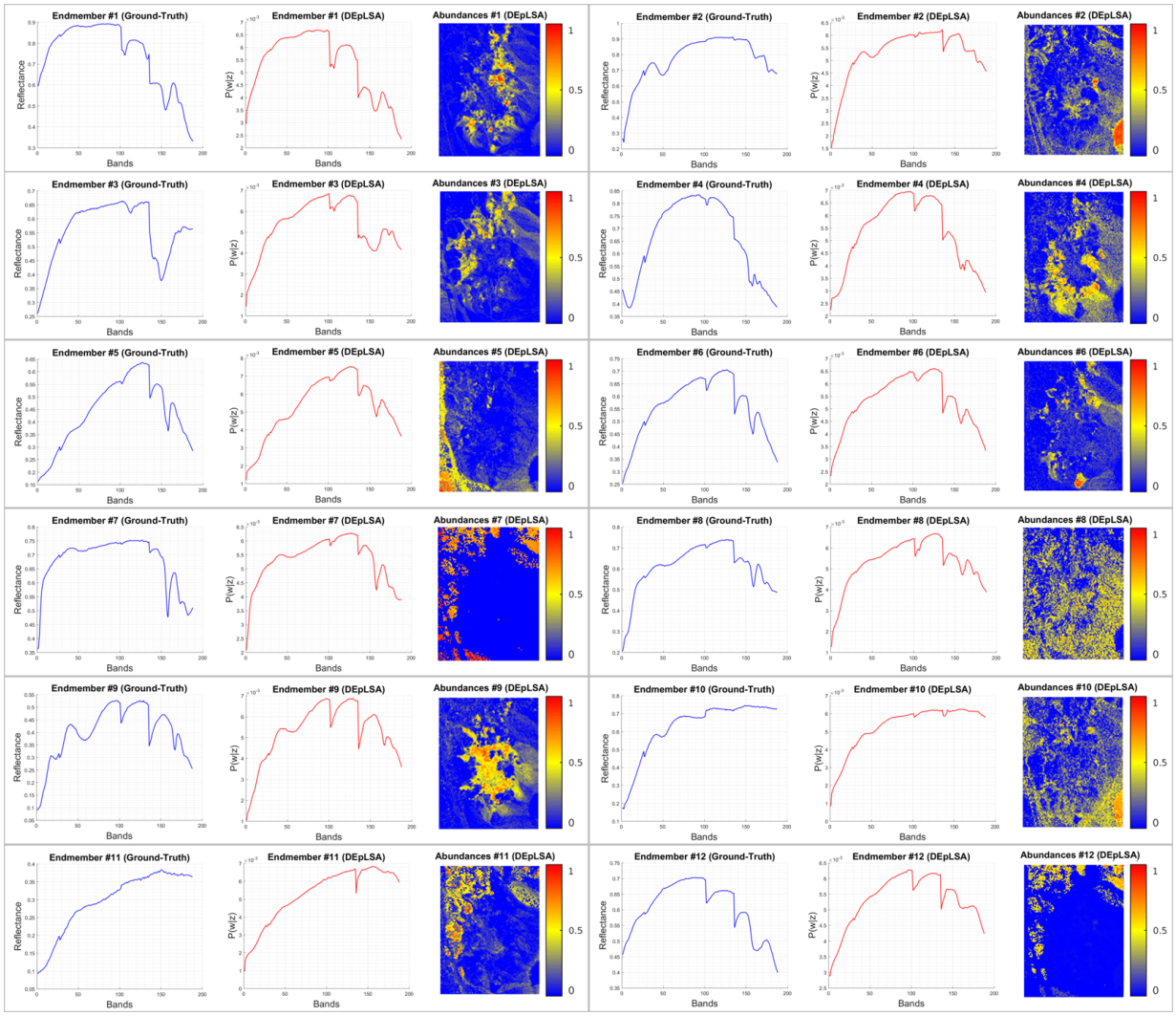

Fig. 9: Cuprite endmember results and abundance maps for the proposed DEpLSA method. For each sub-picture, the first plot shows the ground-truth spectral signature (in blue color), the second one shows the proposed approach endmember estimation (in red) and the last one provides the obtained fractional abundance map.

endmembers.

When analyzing the unmixing results obtained by topic models, several interesting observations can be made. First, the pLSA model clearly shows a better performance for unmixing tasks than LDA. As it was mentioned in Section II, LDA requires an initial estimation of two Dirichlet hyper-parameters and the quality of this estimation may be affected by the number of available documents. In the blind HU application, the number of pixels is constrained to the input image size, and this number is usually rather limited to generate a good initial hyper-parameter estimate for LDA. However, pLSA takes advantage of the use of input pixels as model parameters and, therefore, it is able to extract more accurate semantic patterns using less input information than LDA.

Another important point is related to the use of regularization to relieve the ill-posed nature of the HU

problem. As we can see in Tables I-II, the standard LDA and pLSA models present poor global performance, especially when estimating endmembers. However, a substantial improvement can be reached when introducing sparse regularization terms. The presented results show that pLSA-sp and NMF-sp achieve an important performance improvement over standard models (i.e. pLSA, NMF-div and NMF-mse) by means of considering sparsity constraints on the final estimation of fractional abundancies. In general, sparse regularization is an excellent tool to reduce the uncertainty in the unmixed space [7], and this is precisely the reason why this technique is also effective in topic-based HU.

Overall, VCA and CNMF show good performance in the task of extracting endmembers, and NMF-sp in the task of estimating estimate abundances. Nonetheless the proposed approach is able to provide superior results in both tasks. The abundance maps shown in Section V also support this observation. In the case of the Samson dataset (Fig. 6), soil, tree and water endmembers are represented using pure red, green and blue colors, respectively. As we can see, VCA, CNMF and DEpLSA are the methods that better distinguish among these three endmembers. However, DEpLSA is able to provide a more accurate result. In the coastal area of Fig. 6, VCA and CNMF generate a blurring effect, whereas DEpLSA obtains a result more similar to the ground-truth abundances. In Figs. 7-8, it is also possible to find similar examples to validate the results obtained by the proposed approach. Regarding the Cuprite endmember results provided in Fig. 9, we can also observe that the proposed approach is able to obtain spectral signatures very similar to the corresponding ground-truth endmembers.

A. Performance analysis for different sparsity factors

As it has been commented in Section V-B, the proposed approach δ_d and δ_z sparsity factors have been set to 10^{-2} and 10^{-3}, for all the datasets, in order to use a general configuration. That is, according to the information provided in Section III, these two regularization factors allow us to neglect those small noisy components appearing in $p(z|d)$ and $p(w|z)$ probability distributions throughout the EM optimization process. In order to highlight this point, Figure 10 shows the quantitative assessment for different parameter configuration over the Samson dataset.

Specifically, Figs. 10a-10b provide the SAD and RMSE evaluation when considering δ_d and δ_z within the range $0.00 - 0.04$. In addition, Figs. 10c-10d show the corresponding SAD and RMSE details in the range $0.000 - 0.004$. As we can see in Figs. 10a-10b, the optimal δ_d parameter seems to be between 0.002 and 0.03 for the SAM metric and between 0.00 and 0.02 when considering the RMSE result. Regarding the δ_z parameter, it initially seems not to have a significant impact on the performance, at least for the considered value range. However, the details provided in Figs. 10c-10d reveal that a small regularisation is convenient in both cases.

That is, both the SAD and RMSE details show that there is a small area close to the axis representing $\delta_d = 0$ and $\delta_z = 0$ where the metric performance tends to decrease. Precisely, this effect is produced because tiny probability values, which somehow can be considered noisy in a real scenario, are not regularized in the EM process when considering null sparsity factors. As a result, the proposed approach can take advantage of small regularization factors to increase the resulting performance and this is the reason why we set δ_d and δ_z to 10^{-2} and 10^{-3} as a general settings for all the datasets.

Logically, this configuration may not be optimal for all the considered hyperspectral images, however it pursues to avoid the aforementioned effect while providing the most general scheme. This assertion is also supported by the fact that the proposed approach with the considered configuration is able to outperform the corresponding non-regularized version (DEpLSA-noReg) for all the experiments except for the free-noise synthetic image.

TABLE III: Computational time of unmixing algorithms.

Datasets	K	Time (seconds)				
		VCA	NMF-sp	CNMF	pLSA-sp	DEpLSA
Samson	3	**2.32**	57.99	26.79	5.57	38.46
Jasper	4	**2.70**	38.02	19.81	9.72	52.56
Urban	4	**7.98**	73.32	191.33	77.71	197.10
Cuprite	12	**3.48**	64.00	200.24	85.55	282.70

B. Advantages and limitations of the proposed approach

The main advantage of the proposed DEpLSA-based HU framework lies in the deep-topic structure that it offers to uncover endmembers and abundances. Even though some methods in the literature have tried to use pLSA [27] (or, analogously, NMF [34], [62], [63]) for the unmixing task, they mainly use these models as a straightforward data decomposition process. That is, endmembers and abundances are estimated over the initial spectral space, and this fact limits the semantic potential of topic-models in HU.

The proposed DEpLSA model introduces a new level of topics, called deep-topics (z'), in order to extract the semantic representations of the input spectral data. Then, another level of topics, called restricted-topics (z), is used to uncover the endmembers and abundances over these semantic representations. In this way, the unmixing process is conducted over a semantic representation space, unlike the classical straightforward approach. Additionally, we introduce a dual sparsity constraint over restricted-topics to guarantee regularized solutions.

The underlying rationale behind the improvement provided by DEpLSA is based on its potential to better discern similar spectral patterns in the deep-topic space. Let us explain this concept through a simple visual example. Fig. 11a shows the original Samson data projected onto the two first PCA (Principal Component Analysis) components, where soil, vegetation and water pure pixels are colored in red, green and blue, respectively.

When using pLSA-sp over the original spectral space (Fig. 11b), we can see that pure pixels tend to maintain essentially the same data variability, that is, the extracted topics do not provide any substantial improvement on the data simplex geometry. Nonetheless, the restricted-topic space uncovered by the proposed approach (Fig. 11d) is able to define a clearer geometry over the extracted topics by means of reducing the intra-member variability. In other words, the deep-topic space (Fig. 11c) initially compacts the data that shares the same hidden spectral patterns. Then, the restricted-topic space (Fig. 11d) is able to reduce uncertainty in dense areas of the simplex while maintaining the variability in the less dense parts of it.

Despite the potential of the proposed approach, it still has some limitations which need to be mentioned at this point. Specifically, its computational cost is one of them. Table III shows a summary of the computational time required by VCA, NMF-sp, CNMF, pLSA-sp and DEpLSA unmixing methods over the tested images. As we can see, the proposed model is, on average, the most computationally demanding one and this fact may limit its application.

According to the model relaxation introduced in Section III-A, we can reduce the DEpLSA computational load to a pLSA order cost by using a regular pLSA

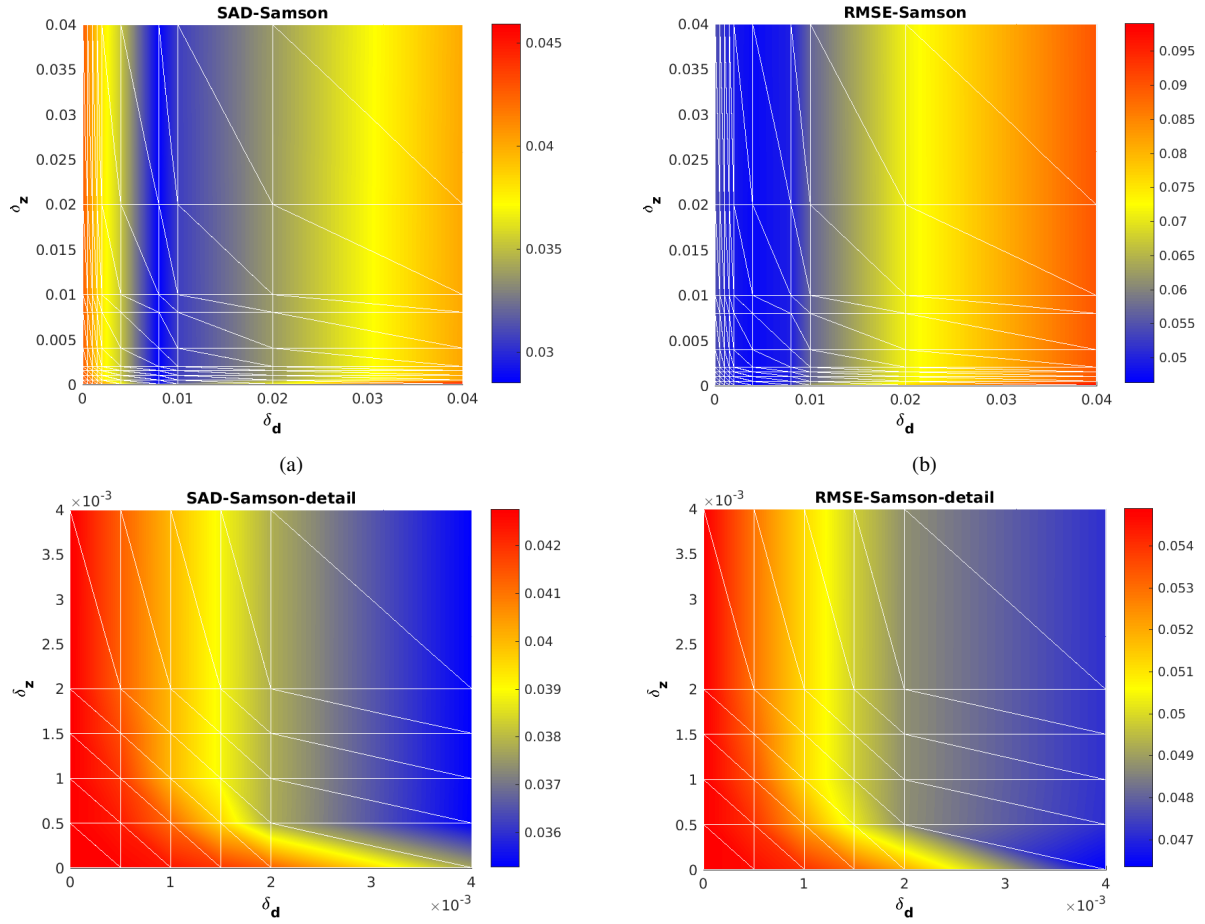

Fig. 10: Result evaluation for Samson datasets using different sparsity factors.

model to estimate the deep-topic space and a regularized pLSA model to uncover the restricted-topic space. However, the computational time that we obtain depends, in practice, on the number of deep-topics, that is $K' = 1000$, which is significantly higher than the number of initial spectral bands (N), i.e. 156, 198, 162 and 188 bands for Samson, Jasper, Urban and Cuprite, respectively. Even though the high dimensionality of the deep-topic space may allow a faster convergence of the model, the total computational time of DEpLSA remains on average 1.3, 2.4 and 3.2 times higher than CNMF, NMF-sp and pLSA-sp costs. At this point, it should be also mentioned the high efficiency of the geometrical method VCA.

Another limitation of the proposed approach is related to the absence of noise on the input image. Even though this may not be an actual limitation in a real-life scenarios because of the inherent complexity of real remotely sensed hyperspectral data, the DEpLSA model has shown a limited performance with the noise-free synthetic data. The proposed approach has been specially designed to deal with the hyperspectral data complexity through the semantic patterns uncovered by the deep-topic space, however the simpler nature of the simulated data makes other straightforward methods more convenient than the proposed approach probabilistic nature.

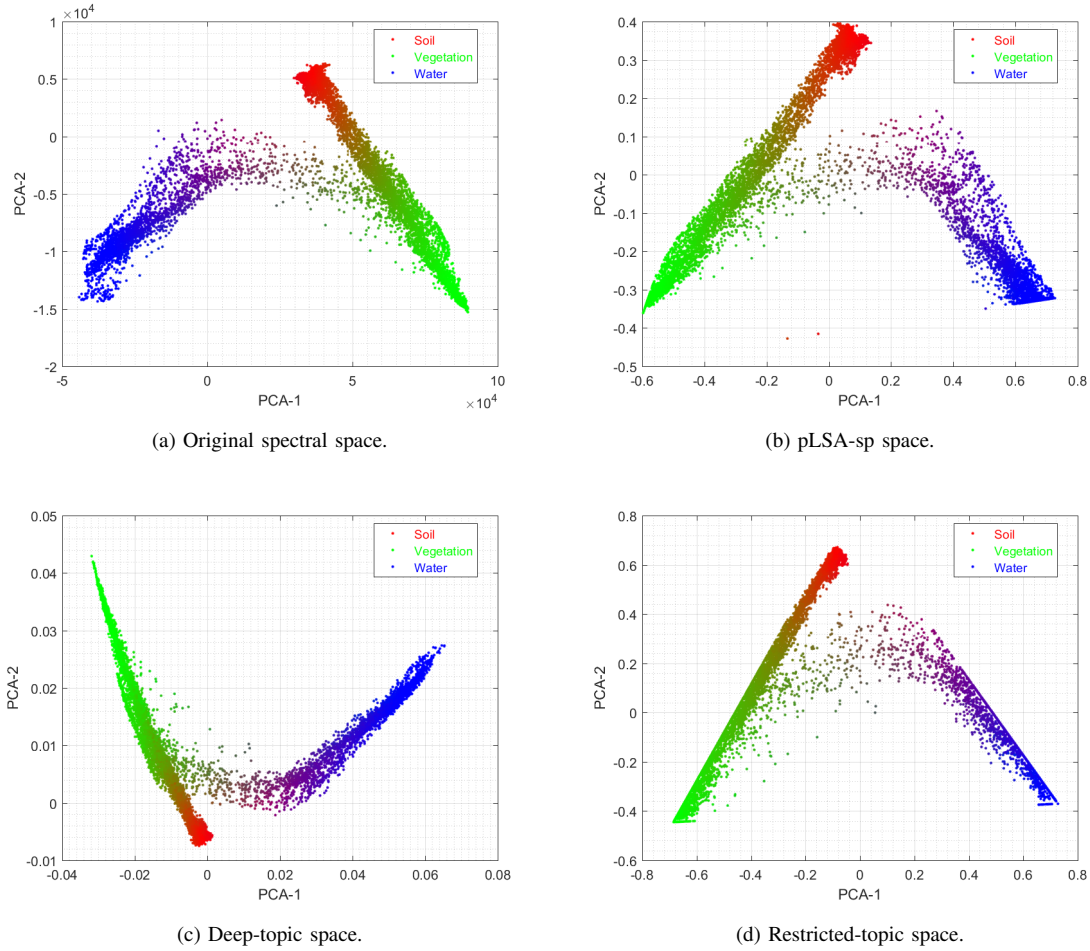

(a) Original spectral space.

(b) pLSA-sp space.

(c) Deep-topic space.

(d) Restricted-topic space.

Fig. 11: Visual representation of Samson data projected onto the two first PCA components.

VII. Conclusions and Future Work

In this work, we have presented a new topic-based unmixing framework specially designed to estimate both endmembers and abundances from remotely sensed hyperspectral imagery. Specifically, we introduce a so-called DEpLSA model in order to deal with the unmixing problem, following a pLSA-based dual-depth architecture. The proposed model generates a first level of deep-topics to extract the semantic representations of the input hyperspectral data. Then, a second level of restricted-topics is computed to estimate endmember spectral signatures and fractional abundances according to the uncovered spectral patterns. Our experimental comparison, conducted using four different hyperspectral datasets, reveals that the proposed approach is able to provide competitive performance with respect to standard topic models, as well as several state-of-the-art unmixing methods available in the literature.

One of the first conclusions that arises from this work is the potential of pLSA-based models to cope with the HU problem. In general, pLSA-based models have shown to obtain better unmixing results than LDA because they can take advantage of the use of spectral pixels as model parameters to generate better topic estimates.

Another important conclusion is related to the use of sparse regularization within the HU field. As the conducted experiments reveal, pLSA and NMF obtain a substantial performance improvement when considering sparsity constraints over spectral signatures and fractional abundances. In a sense, these sparse assumptions help unmixing models to avoid uninformative solutions.

Finally, the most relevant conclusion of the work is related to the effectiveness of the proposed pLSA-based dual-depth architecture to cope with the unmixing problem, especially under real remotely sensed hyperspectral data. Whereas the common algorithm design trend relies on using some models like pLSA as a straightforward data decomposition process, the proposed DEpLSA model transforms this classical perspective into a new probabilistic framework under which the HU process is conducted according to the semantics encapsulated by the deep-topic space.

Although the proposed approach results are encouraging as a HU technique using semantic representations, it still has some limitations which provide room for improvement to conduct more research on topic-based HU. Specifically, our future work is aimed at the following directions: (i) the development of a parallel implementation of the DEpLSA model to significantly reduce its computational time, using graphics processing units (GPUs), (ii) the extension of our model to estimate the ideal sparsity factors for each input image, (iii) the design of automatic procedures to set the most appropriate number of topics in the deep-topic space and (iv) an extension of the proposed HU framework to automatically find the number of endmembers in the original hyperspectral image.

ACKNOWLEDGMENT

This work was supported by the Generalitat Valenciana through the contract APOSTD/2017/007 and by the Spanish Ministry of Economy under projects ESP2016-79503-C2-2-P and TIN2015-63646-C5-5-R. We gratefully thank the Editors and the Anonymous Reviewers for their outstanding comments and suggestions, which greatly helped us to improve the technical quality and presentation of this work.

REFERENCES

[1] A. Plaza, Q. Du, J. M. Bioucas-Dias, X. Jia, and F. A. Kruse, "Foreword to the special issue on spectral unmixing of remotely sensed data," *IEEE Transactions on Geoscience and Remote Sensing*, vol. 49, no. 11, pp. 4103–4110, 2011.

[2] M. T. Eismann, *Hyperspectral Remote Sensing*. SPIE PRESS, 2012.

[3] J. M. Bioucas-Dias, A. Plaza, G. Camps-Valls, P. Scheunders, N. Nasrabadi, and J. Chanussot, "Hyperspectral remote sensing data analysis and future challenges," *IEEE Geoscience and Remote Sensing Magazine*, vol. 1, no. 2, pp. 6–36, 2013.

[4] N. Keshava and J. F. Mustard, "Spectral unmixing," *IEEE Signal Processing Magazine*, vol. 19, no. 1, pp. 44–57, 2002.

[5] W. K. Ma, J. M. Bioucas-Dias, T. H. Chan, N. Gillis, P. Gader, A. J. Plaza, A. Ambikapathi, and C. Y. Chi, "A signal processing perspective on hyperspectral unmixing: Insights from remote sensing," *IEEE Signal Processing Magazine*, vol. 31, no. 1, pp. 67–81, 2014.

[6] D. J. Brady, *Optical Imaging and Spectroscopy*. Wiley, 2009.

[7] J. M. Bioucas-Dias, A. Plaza, N. Dobigeon, M. Parente, Q. Du, P. Gader, and J. Chanussot, "Hyperspectral unmixing overview: Geometrical, statistical, and sparse regression-based approaches," *IEEE Journal of Selected Topics in Applied Earth Observations and Remote Sensing*, vol. 5, no. 2, pp. 354–379, 2012.

[8] J. M. P. Nascimento and J. M. B. Dias, "Vertex component analysis: a fast algorithm to unmix hyperspectral data," *IEEE Transactions on Geoscience and Remote Sensing*, vol. 43, no. 4, pp. 898–910, 2005.

[9] J. Li, A. Agathos, D. Zaharie, J. M. Bioucas-Dias, A. Plaza, and X. Li, "Minimum volume simplex analysis: A fast algorithm for linear hyperspectral unmixing," *IEEE Transactions on Geoscience and Remote Sensing*, vol. 53, no. 9, pp. 5067–5082, 2015.

[10] J. M. P. Nascimento and J. M. Bioucas-Dias, "Hyperspectral unmixing based on mixtures of dirichlet components," *IEEE Transactions on Geoscience and Remote Sensing*, vol. 50, no. 3, pp. 863–878, 2012.

[11] A. Halimi, N. Dobigeon, J. Y. Tourneret, and P. Honeine, "A new bayesian unmixing algorithm for hyperspectral images mitigating endmember variability," in *2015 IEEE International Conference*

on Acoustics, Speech and Signal Processing, 2015, pp. 2469–2473.

[12] M. D. Iordache, J. M. Bioucas-Dias, and A. Plaza, "Sparse unmixing of hyperspectral data," *IEEE Transactions on Geoscience and Remote Sensing*, vol. 49, no. 6, pp. 2014–2039, 2011.

[13] S. Feng, M. F. Duarte, and M. Parente, "Universality of wavelet-based non-homogeneous hidden markov chain model features for hyperspectral signatures," in *IEEE Conference on Computer Vision and Pattern Recognition Workshops*, 2015, pp. 19–27.

[14] Y. Itoh, S. Feng, M. F. Duarte, and M. Parente, "Semisupervised endmember identification in nonlinear spectral mixtures via semantic representation," *IEEE Transactions on Geoscience and Remote Sensing*, vol. 55, no. 6, pp. 3272–3286, 2017.

[15] R. N. Clark, G. A. Swayze, K. E. Livo, R. F. Kokaly, S. J. Sutley, J. B. Dalton, R. R. McDougal, and C. A. Gent, "Imaging spectroscopy: Earth and planetary remote sensing with the usgs tetracorder and expert systems," *Journal of Geophysical Research: Planets*, vol. 108, no. E12, pp. n/a–n/a, 2003, 5131.

[16] Y. Itoh, S. Feng, M. F. Duarte, and M. Parente, "Hyperspectral unmixing via semantic spectral representations," in *IEEE International Midwest Symposium on Circuits and Systems*, 2014, pp. 149–152.

[17] D. M. Blei, "Probabilistic topic models," *Communications of the ACM*, vol. 55, no. 4, pp. 77–84, 2012.

[18] F. Rodrigues, M. Loureno, B. Ribeiro, and F. C. Pereira, "Learning supervised topic models for classification and regression from crowds," *IEEE Transactions on Pattern Analysis and Machine Intelligence*, vol. 39, no. 12, pp. 2409–2422, 2017.

[19] Y. Zhuang, H. Gao, F. Wu, S. Tang, Y. Zhang, and Z. Zhang, "Probabilistic word selection via topic modeling," *IEEE Transactions on Knowledge and Data Engineering*, vol. 27, no. 6, pp. 1643–1655, 2015.

[20] C. Chen, A. Zare, H. N. Trinh, G. O. Omotara, J. T. Cobb, and T. A. Lagaunne, "Partial membership latent dirichlet allocation for soft image segmentation," *IEEE Transactions on Image Processing*, vol. 26, no. 12, pp. 5590–5602, 2017.

[21] Z. Niu, G. Hua, L. Wang, and X. Gao, "Knowledge-based topic model for unsupervised object discovery and localization," *IEEE Transactions on Image Processing*, vol. 27, no. 1, pp. 50–63, 2018.

[22] R. Fernandez-Beltran and F. Pla, "Latent topics-based relevance feedback for video retrieval," *Pattern Recognition*, vol. 51, pp. 72–84, 2016.

[23] W. Luo, H. Li, G. Liu, and L. Zeng, "Semantic annotation of satellite images using author genre topic model," *IEEE Transactions on Geoscience and Remote Sensing*, vol. 52, no. 2, pp. 1356–1368, 2014.

[24] Y. Zhong, Q. Zhu, and L. Zhang, "Scene classification based on the multifeature fusion probabilistic topic model for high spatial resolution remote sensing imagery," *IEEE Transactions on Geoscience and Remote Sensing*, vol. 53, no. 11, pp. 6207–6222, 2015.

[25] Q. Zhu, Y. Zhong, L. Zhang, and D. Li, "Scene classification based on the fully sparse semantic topic model," *IEEE Transactions on Geoscience and Remote Sensing*, vol. 55, no. 10, pp. 5525–5538, 2017.

[26] R. Fernandez-Beltran, P. Latorre-Carmona, and F. Pla, "Latent topic-based super-resolution for remote sensing," *Remote Sensing Letters*, vol. 8, no. 6, pp. 498–507, 2017.

[27] W. Wang and H. Qi, "Unsupervised nonlinear unmixing of hyperspectral images using sparsity constrained probabilistic latent semantic analysis," in *Workshop on Hyperspectral Image and Signal Processing: Evolution in Remote Sensing (WHISPERS)*, 2013, pp. 1–4.

[28] T. Hofmann, "Unsupervised learning by probabilistic latent semantic analysis," *Machine Learning*, vol. 42, no. 1-2, pp. 177–196, 2001.

[29] D. Blei, A. Ng, and M. Jordan, "Latent dirichlet allocation," *Journal of Machine Learning Research*, vol. 3, no. 4-5, pp. 993–1022, 2003.

[30] R. Fernandez-Beltran and F. Pla, "Incremental probabilistic latent semantic analysis for video retrieval," *Image and Vision Computing*, vol. 38, pp. 1–12, 2015.

[31] J. Chang, S. Gerrish, C. Wang, J. L. Boyd-graber, and D. M. Blei, "Reading tea leaves: How humans interpret topic models," in *Advances in Neural Information Processing Systems*, 2009, pp. 288–296.

[32] L. Miao and H. Qi, "Endmember extraction from highly mixed data using minimum volume constrained nonnegative matrix factorization," *IEEE Transactions on Geoscience and Remote Sensing*, vol. 45, no. 3, pp. 765–777, 2007.

[33] A. Huck and M. Guillaume, "Robust hyperspectral data unmixing with spatial and spectral regularized nmf," in *Workshop on Hyperspectral Image and Signals Processing*, vol. 2, 2010, pp. 1–4.

[34] J. Li, J. M. Bioucas-Dias, A. Plaza, and L. Liu, "Robust collaborative nonnegative matrix factorization for hyperspectral unmixing," *IEEE Transactions on Geoscience and Remote Sensing*, vol. 54, no. 10, pp. 6076–6090, 2016.

[35] E. Gaussier and C. Goutte, "Relation between plsa and nmf and implications," in *International ACM SIGIR Conference on Research and Development in Information Retrieval*, 2005, pp. 601–602.

[36] G. McLachlan and D. Peel, *Finite Mixture Models*. Wiley, 2000.

[37] B. Yang, B. Wang, and Z. Wu, "Nonlinear hyperspectral unmixing based on geometric characteristics of bilinear mixture models," *IEEE Transactions on Geoscience and Remote Sensing*, 2017.

[38] A. Marinoni and H. Clenet, "Higher order nonlinear hyperspectral unmixing for mineralogical analysis over extraterrestrial bodies," *IEEE Journal of Selected Topics in Applied Earth Observations and Remote Sensing*, vol. 10, no. 8, pp. 3722–3733, 2017.

[39] A. Halimi, J. M. Bioucas-Dias, N. Dobigeon, G. S. Buller, and S. McLaughlin, "Fast hyperspectral unmixing in presence of nonlinearity or mismodeling effects," *IEEE Transactions on Computational Imaging*, vol. 3, no. 2, pp. 146–159, 2017.

[40] Y. Ma, C. Li, X. Mei, C. Liu, and J. Ma, "Robust sparse hyperspectral unmixing with l2-l1 norm," *IEEE Transactions on Geoscience and Remote Sensing*, vol. 55, no. 3, pp. 1227–1239, 2017.

[41] N. Dobigeon, J.-Y. Tourneret, and C.-I. Chang, "Semi-supervised linear spectral unmixing using a hierarchical bayesian model for hyperspectral imagery," *IEEE Transactions on Signal Processing*, vol. 56, no. 7, pp. 2684–2695, 2008.

[42] K. E. Themelis, A. A. Rontogiannis, and K. D. Koutroumbas, "A novel hierarchical bayesian approach for sparse semisupervised hyperspectral unmixing," *IEEE Transactions on Signal Processing*, vol. 60, no. 2, pp. 585–599, 2012.

[43] Y. Altmann, M. Pereyra, and S. McLaughlin, "Bayesian nonlinear hyperspectral unmixing with spatial residual component analysis," *IEEE Transactions on Computational Imaging*, vol. 1, no. 3, pp. 174–185, 2015.

[44] P. Chen, J. D. Nelson, and J.-Y. Tourneret, "Toward a sparse bayesian markov random field approach to hyperspectral unmixing and classification," *IEEE Transactions on Image Processing*, vol. 26, no. 1, pp. 426–438, 2017.

[45] A. Ertürk, M.-D. Iordache, and A. Plaza, "Sparse unmixing with dictionary pruning for hyperspectral change detection," *IEEE Journal of Selected Topics in Applied Earth Observations and Remote Sensing*, vol. 10, no. 1, pp. 321–330, 2017.

[46] R. Wang, H.-C. Li, A. Pizurica, J. Li, A. Plaza, and W. J. Emery, "Hyperspectral unmixing using double reweighted sparse regression and total variation," *IEEE Geoscience and Remote Sensing Letters*, vol. 14, no. 7, pp. 1146–1150, 2017.

[47] W. Wei, L. Zhang, C. Tian, A. Plaza, and Y. Zhang, "Structured sparse coding-based hyperspectral imagery denoising with intracluster filtering," *IEEE Transactions on Geoscience and Remote Sensing*, vol. 55, no. 12, pp. 6860–6876, 2017.

[48] T. K. Moon, "The expectation-maximization algorithm," *IEEE Signal Processing Magazine*, vol. 13, no. 6, pp. 47–60, 1996.

[49] Y. Zhang, R. Jin, and Z. Zhou, "Understanding bag-of-words model: a statistical framework," *Int. J. Mach. Learn. Cyber.*, vol. 1, no. 1, pp. 43–52, 2010.

[50] J. Plaza, E. M. Hendrix, I. García, G. Martín, and A. Plaza, "On endmember identification in hyperspectral images without pure pixels: A comparison of algorithms," *Journal of Mathematical Imaging and Vision*, vol. 42, no. 2-3, pp. 163–175, 2012.

[51] F. Zhu, Y. Wang, S. Xiang, B. Fan, and C. Pan, "Spectral unmixing via data-guided sparsity," *IEEE Trans. on Image Processing*, vol. 23, no. 12, pp. 5412–5427, 2014.

[52] A. Ertürk, M.-D. Iordache, and A. Plaza, "Sparse unmixing-based change detection for multitemporal hyperspectral images," *IEEE Journal of Selected Topics in Applied Earth Observations and Remote Sensing*, vol. 9, no. 2, pp. 708–719, 2016.

[53] W. He, H. Zhang, and L. Zhang, "Total variation regularized reweighted sparse nonnegative matrix factorization for hyperspectral unmixing," *IEEE Transactions on Geoscience and Remote Sensing*, vol. 55, no. 7, pp. 3909–3921, 2017.

[54] R. Liu, L. Zhang, and B. Du, "A novel endmember extraction method for hyperspectral imagery based on quantum-behaved particle swarm optimization," *IEEE Journal of Selected Topics in Applied Earth Observations and Remote Sensing*, vol. 10, no. 4, pp. 1610–1631, 2017.

[55] V. S. K. Ganesan and V. S, "Maximin distance based band selection for endmember extraction in hyperspectral images using simplex growing algorithm," *Multimedia Tools and Applications*, vol. -, no. -, pp. –, 2017.

[56] "Hypermix toolbox," http://www.hypercomp.es/hypermix, 2016, accessed: 2018-03-12.

[57] "Hyperspectral unmixing datasets and ground truths," http://www.escience.cn/people/feiyunZHU/Dataset_GT.html, 2016, accessed: 2018-01-05.

[58] F. Zhu, Y. Wang, S. Xiang, B. Fan, and C. Pan, "Structured sparse method for hyperspectral unmixing," *ISPRS Journal of Photogrammetry and Remote Sensing*, vol. 88, pp. 101–118, 2014.

[59] F. Zhu, Y. Wang, B. Fan, G. Meng, and C. Pan, "Effective spectral unmixing via robust representation and learning-based sparsity," *CoRR*, vol. abs/1409.0685, 2014.

[60] Y. Wang, C. Pan, S. Xiang, and F. Zhu, "Robust hyperspectral unmixing with correntropy-based metric," *IEEE Transactions on Image Processing*, vol. 24, no. 11, pp. 4027–4040, 2015.

[61] D. D. Lee and H. S. Seung, "Learning the parts of objects by nonnegative matrix factorization," *Nature*, vol. 401, pp. 788–791, 1999.

[62] ——, "Algorithms for non-negative matrix factorization," in *Proceedings of Neural Information Processing Systems*, 2000, pp. 556–562.

[63] P. O. Hoyer, "Non-negative matrix factorization with sparseness constraints," *J. Mach. Learn. Res.*, vol. 5, pp. 1457–1469, 2004.

[64] J. M. Bioucas-Dias and J. M. P. Nascimento, "Hyperspectral subspace identification," *IEEE Transactions on Geoscience and Remote Sensing*, vol. 46, no. 8, pp. 2435–2445, 2008.

[65] R. H. Yuhas, G. A. F. H., and B. J. W., "Discrimination among semi-arid landscape endmembers using the spectral anglemapper

(sam) algorithm," in *Proc. Summaries 3rd Annu. JPL Airborne Geosci. Workshop*, 1992, pp. 147–149.

[66] F. Zhu, "Spectral unmixing datasets with ground truths," *arXiv preprint arXiv:1708.05125*, 2017.

[67] S. Jia and Y. Qian, "Spectral and spatial complexity-based hyperspectral unmixing," *IEEE Transactions on Geoscience and Remote Sensing*, vol. 45, no. 12, pp. 3867–3879, 2007.

[68] ——, "Constrained nonnegative matrix factorization for hyperspectral unmixing," *IEEE Transactions on Geoscience and Remote Sensing*, vol. 47, no. 1, pp. 161–173, 2009.

[69] C.-I. Chang and Q. Du, "Estimation of number of spectrally distinct signal sources in hyperspectral imagery," *IEEE Transactions on geoscience and remote sensing*, vol. 42, no. 3, pp. 608–619, 2004.